Reconfigurable Acoustic Multiplexer/Demultiplexer Using Time Division

Amir Darabi, Emily Kliewer, Michael J. Leamy*
Woodruff School of Mechanical Engineering, Georgia Institute of Technology,
771 Ferst Drive N.W., Atlanta, GA, 30332, USA.

ABSTRACT

Implementing guided-wave technologies in mechanical systems has always been a significant challenge due to losses associated with defects and sharp angles. Inspired by quantum Hall effects in condensed matter physics, mechanical topological insulators (TIs) have recently addressed these issues using efficient and robust signal transport supported by backscattering-immune topological protection. In this Letter we demonstrate the first mechanical TI-based multiplexer/demultiplexer using acoustic waves. Triangular arrays of circular piezoelectric disks bonded to an aluminum host medium, shunted through external circuits with equivalent negative capacitance, break inversion symmetry and create topologically-protected interface states. Combined with programmable switches, the device enables acoustic waves to travel efficiently from an input source to multiple output receivers, or vice-versa, via dynamic topological interfaces. The proposed acoustic multiplexer/demultiplexer is envisioned to find application in wave-based devices, as an accompaniment to ubiquitous surface acoustic wave (SAW) filtering used in communication devices such as cell phones, radios, and computer peripherals.

*Author to whom correspondence should be addressed: michael.leamy@me.gatech.edu

The challenge of propagating lossless information has been readdressed in the past few years through introduction of topological insulators (TIs) supporting topologically-protected states. These advantageous states, induced by quantum Hall and quantum spin Hall effects, or their analogs, originated from electronic materials using Fermi-Dirac statistics [1, 2], then appeared in classical waves in electromagnetic systems [3–6], and most recently in phononic systems [7–9]. These structures have a unique potential to protect propagating waves against backscattering in the presence of sharp edges, disorder, and defects over broad frequency ranges [10, 11].

Recently, mechanical TIs have been explored to control phonons in statical states [7, 12] or dynamical waves [8, 13] with minimal diffraction losses. As compared to photonic systems at the same excitation frequency, mechanical systems have the benefit of operating at smaller wavelengths with stronger boson-boson interactions [14]. Mechanical TIs can be categorized into two main quantum-analogous groups. The first group mimics the quantum Hall effect (QHE) by breaking time-reversal symmetry in any of a number of demonstrated ways, such as employing Lorentz forces [15], gyroscopes or rotating frames [16, 17], or spatio-temporal control of material properties (e.g., elasticity) [18, 19]. The second group mimics the quantum spin Hall effect (QSHE) by breaking the inversion symmetry in a passive manner, featuring both forward and backward-propagating edge modes, without the need of external energy input [8, 10, 20]. These *passive* devices have been explored numerically and tested experimentally for both discrete systems composed of masses and springs [8, 18, 21, 22], and elastic waves propagating in thin plates [10, 23]. However, due to the need for pairs of coincident Dirac cones in QSHE, complexities arise in designing and fabricating a functional QSHE-based TI. To address this issue, TIs based on the quantum valley Hall effect (QVHE) have recently been introduced which break inversion symmetry in a simpler fashion, requiring only one set of degenerate Dirac cones [24–27]. Similar to other types of TIs, QVHE has been extended to phononic systems to demonstrate valley interface states [28] by utilizing: i) anisotropic scatterers in sonic crystals [29], ii) arrays of resonators or different inclusion types in thin plates [30–32], and iii) shunted piezoelectric patches with external negative capacitance [11, 33, 34].

In order to realize the full potential of mechanical topological insulators in commercial applications, it is highly desirable that they be reconfigurable and programmable such that guided waves propagate along dynamic pathways with minimal diffraction loss. Recently Darabi *et al.* [33] proposed and experimentally tested a programmable electroacoustic TI in which a thin plate supports a periodic array of switched piezoelectric (PZT) patches connected to negative capacitance circuits. By employing two PZTs per unit cell, and switching on one or the other (yielding material A and B type, respectively), dramatic stiffness changes local to the PZT can be introduced, which in turn breaks inversion symmetry. Topological states then exist anytime the two material types form an interface.

In this Letter we build upon the electroacoustic system introduced in [33] and report the first TI-based mechan-

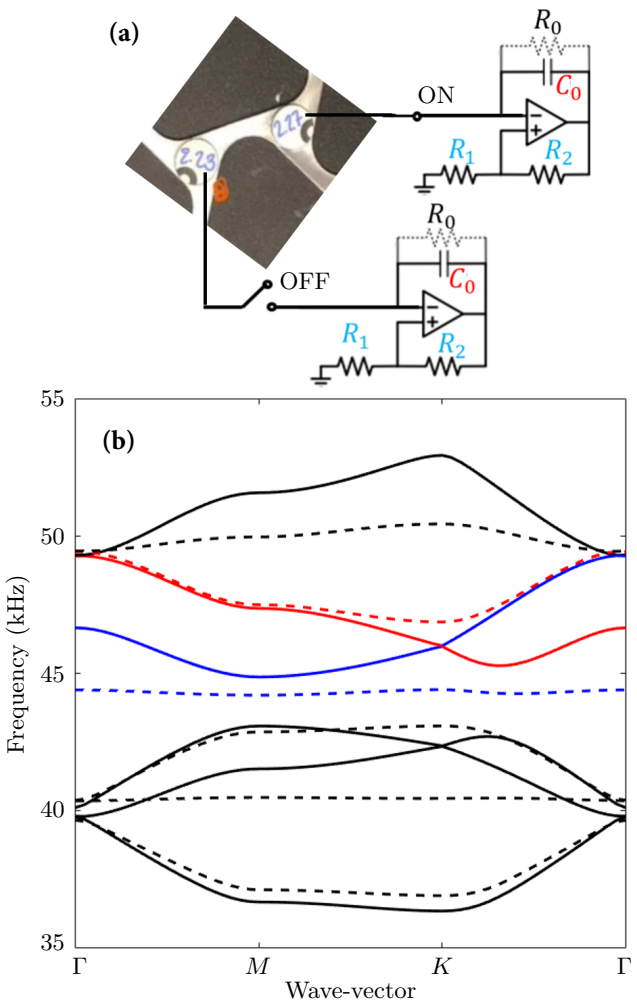

FIG. 1. **Inversion symmetry breaking in the proposed triangular unit cell. (a)** Schematic of a 1 mm thick aluminum triangular unit cell attached to two cylindrical piezoelectric (PZT) disks, each with thickness 0.7 mm and diameter $d_1 = 15$ mm. Attached shunted circuits provide negative capacitance $C' = -(R_2C_0)/R1$, which alter the stiffness of the PZTs, where R_1, R_2 are resistors (marked in blue), and C_0 is a capacitor (marked in red). Each of these circuits also includes an op-amp, a resistor to prevent saturation of the capacitor (R_0), and two switches to connect/disconnect the circuit from the disks. **(b)** Comparison between the band structures along the edges of the irreducible Brillouin zone when both of the switches are OFF (solid-curves with a clear Dirac point at ≈ 46 kHz) and when one of them is ON (dashed-curves with a clear topologically protected bandgap from approximately 44 to 48 kHz). Blue and red solid/dashed lines represent branches bounding the region of interest (i.e., the topological bandgap) while black lines depict other branches.

ical multiplexer/demultiplexer, where the topological interfaces needed for propagating waves can alternate in real time simply by controlling the PZT switches. This is achieved by adding a controller to the setup which opens and closes switches connecting the PZTs to the external circuits. We use a spatial implementation of multiplexing on a fixed frequency, which is commonly termed "time-division multiplexing" [35]. The definition of multiplexing in this paper differs from "frequency-division multiplexing," which uses multiple frequency bands to multiplex over a single channel. Here, waves are guided from input(s) to output(s) with minimal loss and topological protection from backscattering. We believe the proposed mechanical multiplexer/demultiplexer can be a stepping stone towards mechanical channeling of information to complement widely-used mechanical filters (e.g., SAW devices) in communication devices, radios, and computer peripherals.

The proposed system for multiplexing and demultiplexing consists of periodically repeated triangular unit cells each formed by two shunted PZT disks bonded to a host aluminum plate. With both switches open, the lattice supports Dirac points. Closing either switch breaks inversion symmetry, in turn creating a bandgap located at the original Dirac point and supporting topologically protected states. Figure 1**(a)** depicts the 1 mm thick graphene-like unit cell studied in this Letter, which is composed from an aluminum plate and two shunted piezoelectric patches having diameter and thickness of 15 mm and 0.7 mm, respectively. Each PZT disk connects to a circuit (also shown in Fig. 1**(a)**) with an equivalent negative capacitance through an external ON/OFF switch. These circuits are composed of an operational amplifier (op-amp), two resistors connected in series ($R_1 = 100$ ohm, $R_2 = 150$ ohm), and one capacitor ($C_0 = 1.7$ nF) to provide a negative capacitance of $C_{neg} = -C_0R_2/R_1$. These unit cells are then periodically repeated in the lattice directions to form the proposed structure. Solid lines in Fig. 1**(b)** represent the band structure of this unit cell when both of PZT disks experience open circuit conditions (i.e., both switches are off). As illustrated, two connected Dirac cones present at the $K-$point (at approximately $f = 46$ kHz), where two of the bands (one in blue and one in red) cross transversely.

Setting one of the PZT switches to ON, with the other one OFF, breaks inversion symmetry in the unit cell and separates the folded Dirac cones for the frequency range of interest ($40 - 50$ kHz for this study). This connects the PZT (e.g., the green one) to the external negative capacitance circuit, which provides a significant change in the elastic modulus of the disk [36–38]. The band-structure of the broken-symmetry unit cell is plotted in Fig. 1**(b)** as dashed lines, documenting a clear topological bandgap (bounded with red and blue dashed lines), at the location of the original Dirac point, extending from approximately 44 kHz to 48 kHz. Each band surrounding the bandgap has a valley Chern number of $\pm 1/2$, providing the total Chern number of ($|\Delta C_v| = 1$) [39] at the intersection of two sub-structures with opposite circuit conditions. Please refer to Darabi *et al.* [33] for a full discussion on the computation of Chern numbers

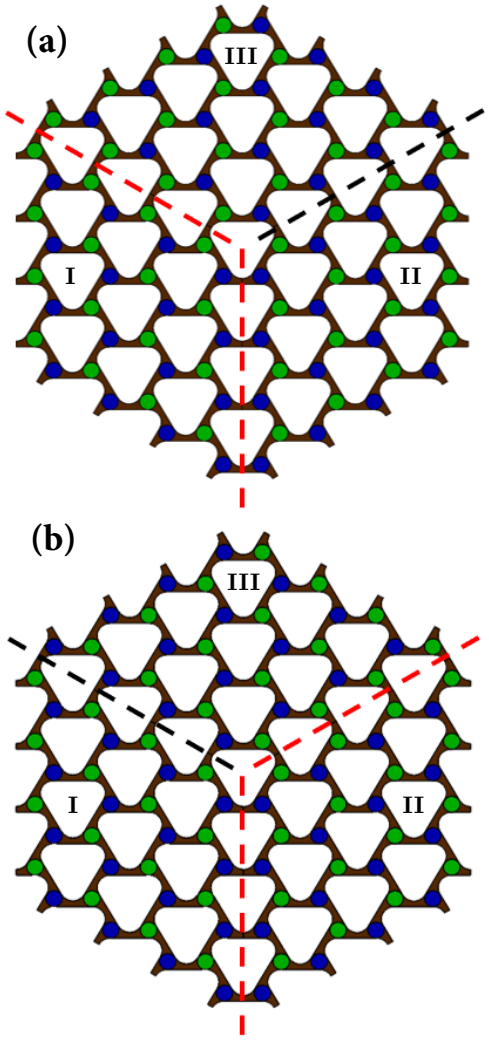

FIG. 2. **Schematic of the proposed multiplexing and demultiplexing device.** The device is composed of three subdomains, each composed of an array of 4×4 unit cells. In the two sub-figures, blue disks depict PZTs disconnected from their circuits, and green disks depict PZTs connected to their external circuits. **(a)** Operation in which subdomain III experiences the same symmetry condition as subdomain II. **(b)** Operation in which subdomain III experiences the same condition as subdomain I. For both subfigures, red dashed-lines represent a topological interface supporting wave propagation, and black dashed-lines represent boundaries between two domains with identical symmetry.

and details for generating the band-structure.

A particularly intriguing property of topological insulators is their ability to guide waves along sharp-edged trajectories free of backscattering and with minimal loss. For mechanical systems, this unique behavior has significant implications for designing acoustic multiplexing and demultiplexing devices to complement, for example, mechanical filters in communication-based devices. Such devices are configured next using the electroacuoustic material described above.

As depicted in Fig. 2, we consider a system composed of three subdomains, each with sixteen unit cells periodically repeated in the two lattice directions. The subdomain interfaces are separated by an angle of 120 degree, which is convenient for getting the largest separation of the signals. For the subdomain labeled as I, the disks on the lower half of the unit cells are always shunted and the rest are disconnected, while for subdomain II, the disks on the upper half of the unit cell are always shunted and the rest are disconnected. This creates a topological interface between these two subdomains (marked with vertical red dashed line) supporting backscattering immune interface waves at a frequency within the topological bandgap. On the contrary, for subdomain III, all the disks are shunted to external circuits, but only half of the connecting switches are ON, and the other half are OFF. Therefore, the symmetry condition of subdomain III can alternate between experiencing the same condition as either subdomain I or II, yielding dynamic interfaces connecting either the top-left port to the bottom port (see Fig. 2**(a)**) or the top-right port to the bottom port (see Fig. 2**(b)**). This then enables multiplexing in which two input ports (i.e., top-left and top-right) channel information to a single output port (i.e., bottom), or demultiplexing in which one input port (i.e., bottom) channels information to two output ports (i.e., top-left and top-bottom).

The operation described above requires 32 controllable single-pole switches, or 16 controllable double-pole switches, to alternate subdomain III between the two requisite symmetry types. In practical implementation, since an unpowered op-amp acts as on open switch, only two controllable single-pole switches (or one controllable double-pole switch) are needed if each switch is used to power ON/OFF all of the op-amps associated with the top and bottom unit cell PZTs, respectively. No physical switches are then needed between the PZTs and the shunted circuits. This is the strategy pursued in the experiments described next.

Figure 3 depicts the fabricated structure (on the left) and the external circuit (on the right). This structure is realized by machining a 1 mm thickness aluminum plate ($E = 70\ GPa$, $\rho = 2700\ kg/m^3$, $\nu = 0.33$) and bonding (using 3M DP270 Epoxy Adhesive) 96 piezoelectric disks. Each piezoelectric disk has a 15 mm diameter and a 0.7 mm thickness. For each circuit wired to the PZT disks, negative capacitance $C' = -2.55\ nf$ is obtained by using $R_1 = 100, R_2 = 150\ \Omega$, $C_0 = 1.7\ nF$, and $R_0 = 1\ M\Omega$. A Polytec PSV-400 scanning laser Doppler vibrometer measures the resulting out-of-plane wavefield velocity using the backside of the aluminum plate, repeating and averaging each measurement 10 times (in order to reduce the influence of noise). In order to generate waves into the system, one of the bonded piezoelectric disks is connected to a $150mV$ (peak-to-peak) burst sinusoidal signal, using a function generator (Agilent 33220A)

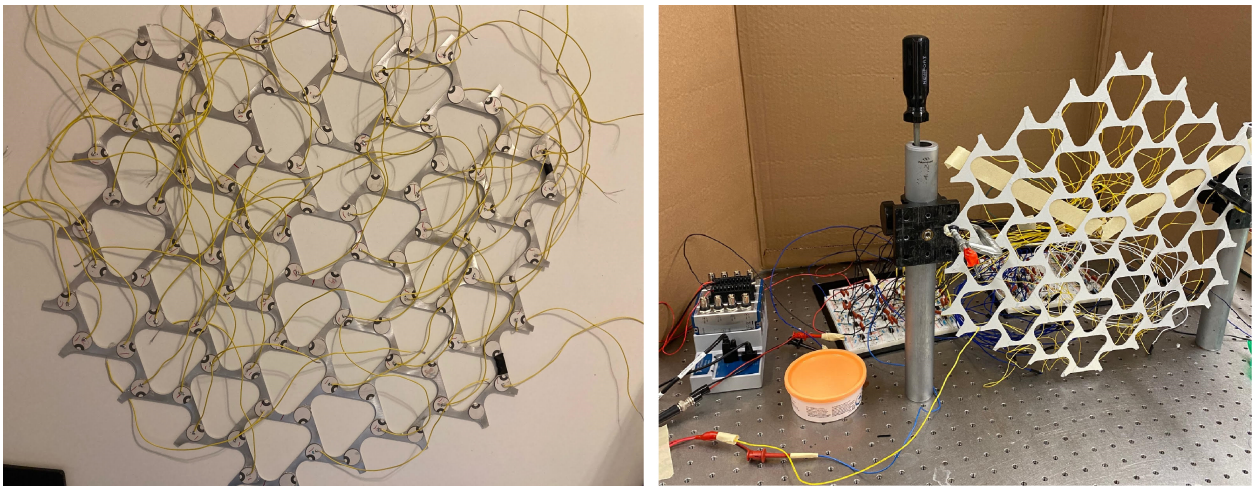

FIG. 3. Fabricated experimental setup.

coupled to a voltage amplifier (B&K1040L). Finally, in order to decrease the boundary effects at the location of the source, absorbing patches are used to reduce the leakage of propagation waves on the edge. In order to find the bandgap experimentally, first one point falling on the intended interface between two opposite domains is considered. While all the OP-AMPs are off (i.e, the PZTs are not connected to a negative capacitance circuit), a frequency sweep for the response of the system at the considered point is performed. For this condition, all the interfaces disappear (no symmetry is broken); hence no bandgaps should be reported. This test is repeated again while the symmetry is broken (by turning ON the corresponding OP-AMPs), in which a new frequency response for a system with a topological bandgap is achieved. By comparing the response of these two tests, the frequency range of interest containing the topological bandgap can be obtained.

Figure 4 displays the full-field response of the system over time for a source located at the bottom of the structure (marked with a green star). First, we use the source to send sinusoidal signals at 54 kHz while powering half of the op-amps such that subdomain III's symmetry condition matches subdomain I's. Due to the approximate nature of the computational model, the topological bandgap in the fabricated structure appears at a higher frequency than that predicted by the model. As documented in Fig. 4, the signal propagates from the source to the first receiver (marked with a red star on the top-right corner) along the introduced topological interface connecting separating subdomains I-II and II-III, bending towards the receiver with little to no backscattering. After the intended signal packet reaches the first receiver at $t = 1.5\ ms$, we pause the system for 1.5 ms to allow the waves to be fully absorbed, preparing the structure for the second signal packet. Then at time $t = 3\ ms$, we send an additional ten cycles to the source, this time with subdomain III's symmetry condition matching subdomain II's. The signal travels along the new interface separating subdomains I-II and I-III, reaching the second receiver at the left corner at $t = 4.5\ ms$. Repeating the operation periodically allows continuous operation in which two multiplexed signals arriving at the same input (and spaced in time) are separated into two channels, effectively demonstrating demultiplexing of information. Reverse operation allows for multiplexing.

To further illustrate the effectiveness of the demultiplexing device, we plot in Fig. 5 the signal transmission ratio as a function of time at both receivers (i.e., both output channels). As documented, the signal amplitude at the first receive reaches its maximum at approximately time $t = 1.5\ ms$, with 75 percent of the sending signal amplitude recovered. Similarly, the signal at the second receiver reaches its maximum amplitude (80 percent of the source signal) at approximately time $t = 5\ ms$. Note that the signal strength at the first output channel is minimal when the second output channel signal strength is maximal, and vice-versa.

In conclusion, this Letter reports the first design and experimental implementation of a reconfigurable mechanical topological insulator operating as an efficient multiplexer or demultiplexer. By employing three locations for transmitter/receivers and a set of controllable switches, (periodic) dynamic topological interfaces are introduced which direct information sequentially from an input to two outputs (demultiplexing), or from two inputs to an output (multiplexing). Based on the channeling concept presented, together with widely-used SAW filtering devices, it may be possible to develop a single mechanical platform which accomplishes the two fundamental communication operations (filtering and channelling) using inexpensive components which avoid high battery usage associated with digital means, such as digital signal processing. The presented concept may also

find use in hazardous or harsh environments (e.g., high temperature or high dynamic loads) problematic for traditional computing-based solutions.

Funding: This work was supported by the National Science Foundation with grants No. 1929849 and No. 1741565. **Author Contributions**: AD, ML conceived the idea. AD and EK designed and fabricated the structure under the supervision of ML. All authors contributed in writing the manuscript. **Data Availability**: All data needed to evaluate the conclusions in the paper are present in the paper. Additional data related to this paper may be requested from the authors. **Competing interests**: All authors declare that they have no competing interests.

[1] C. L. Kane and E. J. Mele, Quantum spin hall effect in graphene, Physical review letters **95**, 226801 (2005).
[2] M. Z. Hasan and C. L. Kane, Colloquium: topological insulators, Reviews of Modern Physics **82**, 3045 (2010).
[3] F. Haldane and S. Raghu, Possible realization of directional optical waveguides in photonic crystals with broken time-reversal symmetry, Physical review letters **100**, 013904 (2008).
[4] A. B. Khanikaev, S. H. Mousavi, W.-K. Tse, M. Kargarian, A. H. MacDonald, and G. Shvets, Photonic topological insulators, Nature materials **12**, 233 (2013).
[5] M. Hafezi, S. Mittal, J. Fan, A. Migdall, and J. Taylor, Imaging topological edge states in silicon photonics, Nature Photonics **7**, 1001 (2013).
[6] A. B. Khanikaev and G. Shvets, Two-dimensional topological photonics, Nature Photonics **11**, 763 (2017).
[7] J. Paulose, B. G.-g. Chen, and V. Vitelli, Topological modes bound to dislocations in mechanical metamaterials, Nature Physics **11**, 153 (2015).
[8] R. Süsstrunk and S. D. Huber, Observation of phononic helical edge states in a mechanical topological insulator, Science **349**, 47 (2015).
[9] R. Fleury, D. L. Sounas, C. F. Sieck, M. R. Haberman, and A. Alù, Sound isolation and giant linear nonreciprocity in a compact acoustic circulator, Science **343**, 516 (2014).
[10] M. Miniaci, R. Pal, B. Morvan, and M. Ruzzene, Experimental observation of topologically protected helical edge modes in patterned elastic plates, Physical Review X **8**, 031074 (2018).
[11] A. Darabi, X. Ni, M. Leamy, and A. Alù, Reconfigurable floquet elastodynamic topological insulator based on synthetic angular momentum bias, Science advances **6**, eaba8656 (2020).
[12] C. Kane and T. Lubensky, Topological boundary modes in isostatic lattices, Nature Physics **10**, 39 (2014).
[13] T. Kariyado and Y. Hatsugai, Manipulation of dirac cones in mechanical graphene, Scientific reports **5**, 18107 (2015).
[14] A. B. Khanikaev, R. Fleury, S. H. Mousavi, and A. Alù, Topologically robust sound propagation in an angular-momentum-biased graphene-like resonator lattice, Nature communications **6**, 8260 (2015).
[15] E. Prodan and C. Prodan, Topological phonon modes and their role in dynamic instability of microtubules, Physical review letters **103**, 248101 (2009).
[16] P. Wang, L. Lu, and K. Bertoldi, Topological phononic crystals with one-way elastic edge waves, Physical review letters **115**, 104302 (2015).
[17] L. M. Nash, D. Kleckner, A. Read, V. Vitelli, A. M. Turner, and W. T. Irvine, Topological mechanics of gyroscopic metamaterials, Proceedings of the National Academy of Sciences **112**, 14495 (2015).
[18] R. Chaunsali, E. Kim, A. Thakkar, P. G. Kevrekidis, and J. Yang, Demonstrating an in situ topological band transition in cylindrical granular chains, Physical review letters **119**, 024301 (2017).
[19] R. Fleury, A. B. Khanikaev, and A. Alu, Floquet topological insulators for sound, Nature communications **7**, 11744 (2016).
[20] S. H. Mousavi, A. B. Khanikaev, and Z. Wang, Topologically protected elastic waves in phononic metamaterials, Nature communications **6**, 8682 (2015).
[21] S. D. Huber, Topological mechanics, Nature Physics **12**, 621 (2016).
[22] E. Prodan, K. Dobiszewski, A. Kanwal, J. Palmieri, and C. Prodan, Dynamical majorana edge modes in a broad class of topological mechanical systems, Nature communications **8**, 14587 (2017).
[23] R. Chaunsali, C.-W. Chen, and J. Yang, Subwavelength and directional control of flexural waves in zone-folding induced topological plates, Physical Review B **97**, 054307 (2018).
[24] A. Rycerz, J. Tworzydo, and C. Beenakker, Valley filter and valley valve in graphene, Nature Physics **3**, 172 (2007).
[25] F. Zhang, J. Jung, G. A. Fiete, Q. Niu, and A. H. MacDonald, Spontaneous quantum hall states in chirally stacked few-layer graphene systems, Physical review letters **106**, 156801 (2011).
[26] K. F. Mak, K. L. McGill, J. Park, and P. L. McEuen, The valley hall effect in mos2 transistors, Science **344**, 1489 (2014).
[27] J.-W. Dong, X.-D. Chen, H. Zhu, Y. Wang, and X. Zhang, Valley photonic crystals for control of spin and topology, Nature materials **16**, 298 (2017).
[28] J. Lu, C. Qiu, M. Ke, and Z. Liu, Valley vortex states in sonic crystals, Physical review letters **116**, 093901 (2016).
[29] J. Lu, C. Qiu, L. Ye, X. Fan, M. Ke, F. Zhang, and Z. Liu, Observation of topological valley transport of sound in sonic crystals, Nature Physics **13**, 369 (2017).
[30] R. K. Pal and M. Ruzzene, Edge waves in plates with resonators: an elastic analogue of the quantum valley hall effect, New Journal of Physics **19**, 025001 (2017).
[31] J. Vila, R. K. Pal, and M. Ruzzene, Observation of topological valley modes in an elastic hexagonal lattice, Physical Review B **96**, 134307 (2017).
[32] A. Darabi and M. J. Leamy, Reconfigurable topological insulator for elastic waves, The Journal of the Acoustical Society of America **146**, 773 (2019).
[33] A. Darabi, M. Collet, and M. J. Leamy, Experimental realization of a reconfigurable electroacoustic topological insulator, Proceedings of the National Academy of Sciences **117**, 16138 (2020).
[34] H. Benndorf, Über einen plattenkondensator mit negativer kapazität, Zeitschrift für Physik **82**, 397 (1933).

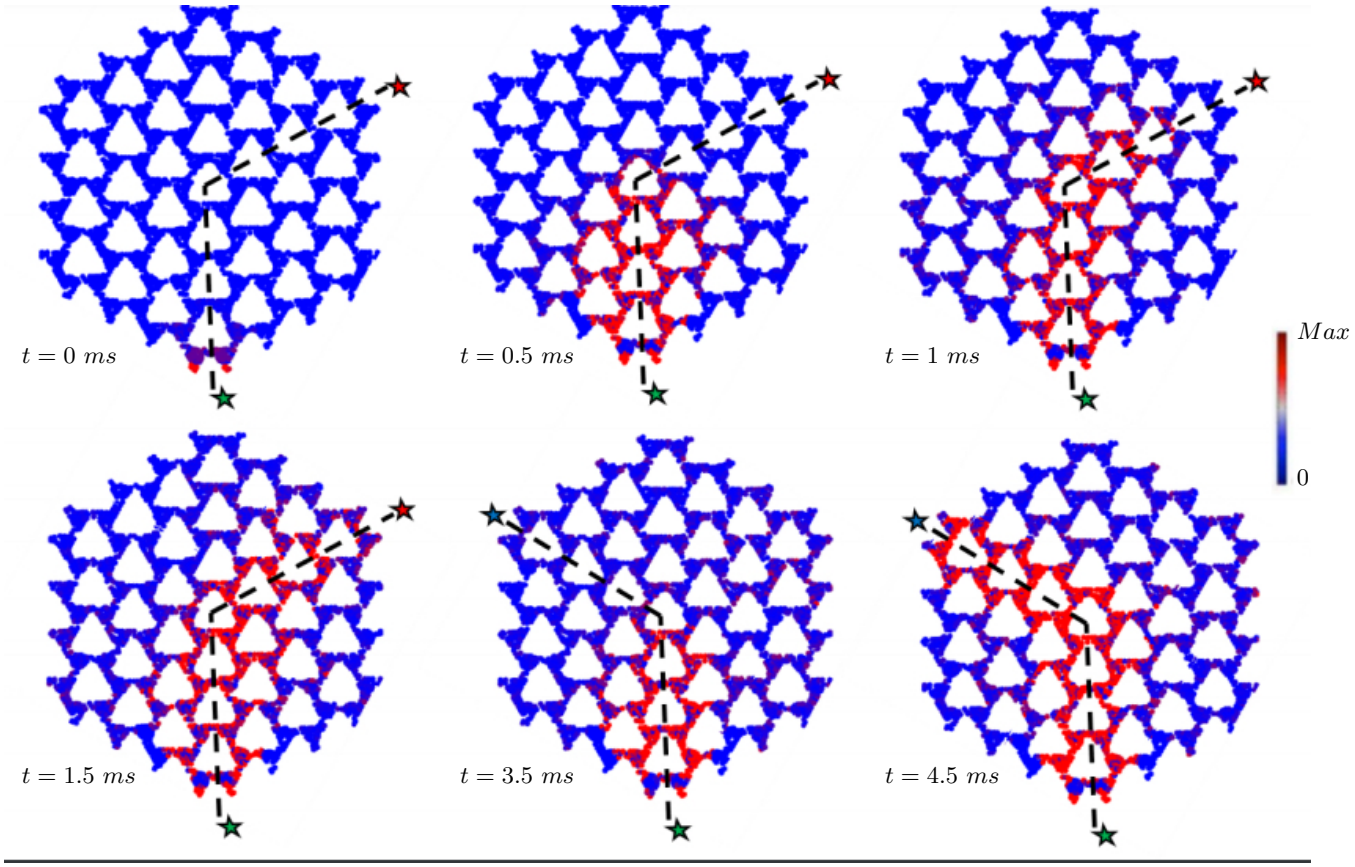

FIG. 4. **Experimentally-characterized demultiplexing operation.** Experimentally-measured full-field response when the device is excited at 54 kHz documenting wave propagation along dynamic interfaces with minimal loss, thus achieving demultiplexing. All displacements have been normalized to the amplitude of the input wave.

[35] D. M. Spirit, A. D. Ellis, and P. E. Barnsley, Optical time division multiplexing: Systems and networks, IEEE Communications Magazine **32**, 56 (1994).

[36] S. Behrens, A. Fleming, and S. Moheimani, A broadband controller for shunt piezoelectric damping of structural vibration, Smart materials and structures **12**, 18 (2003).

[37] B. S. Beck, K. A. Cunefare, and M. Collet, The power output and efficiency of a negative capacitance shunt for vibration control of a flexural system, Smart Materials and Structures **22**, 065009 (2013).

[38] N. W. Hagood and A. von Flotow, Damping of structural vibrations with piezoelectric materials and passive electrical networks, Journal of Sound and Vibration **146**, 243 (1991).

[39] Y. Hatsugai, Chern number and edge states in the integer quantum hall effect, Physical review letters **71**, 3697 (1993).

[40] B. De Marneffe and A. Preumont, Vibration damping with negative capacitance shunts: theory and experiment, Smart Materials and Structures **17**, 035015 (2008).

[41] G. Trainiti, Y. Xia, J. Marconi, G. Cazzulani, A. Erturk, and M. Ruzzene, Time-periodic stiffness modulation in elastic metamaterials for selective wave filtering: Theory and experiment, Physical review letters **122**, 124301 (2019).

[42] H. C. P. Adrian, *Electronic Band Structure in Topological Textures*, Ph.D. thesis, The Chinese University of Hong Kong (2011).

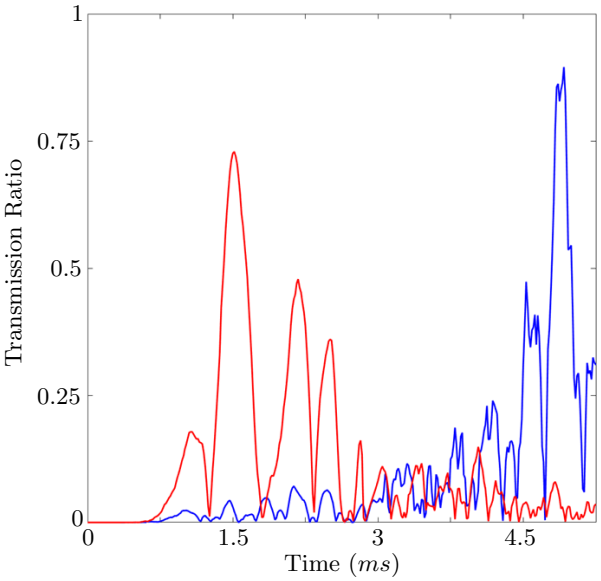

FIG. 5. **Experimentally-measured transmission ratio at both receivers.** Experimentally measured transmission ratio of the two outputs (marked with blue and red stars in Fig. 4) over time, excited by a 54 kHz source (marked with a green star in Fig. 4). The red and blue curves capture the wave amplitude at the first (marked with a red star) and second (marked with a blue star) receivers, respectively. All displacements have been normalized to the amplitude of the input wave at the source.